Effect of membrane composition on DivIVA-membrane interaction

Jurásek, Miroslav; Flärdh, Klas; Vácha, Robert

Published in:
Biochimica et Biophysica Acta - Biomembranes

DOI:
10.1016/j.bbamem.2019.183144

2020

Document Version:
Peer reviewed version (aka post-print)

Effect of membrane composition on DivIVA-membrane interaction

Miroslav Jurásek[a], Klas Flärdh[b] and Robert Vácha[a,c,*]

[a]Faculty of Science, Masaryk University, Kamenice 753/5, 625 00 Brno, Czech Republic
[b]Department of Biology, Lund University, Sölvegatan 35, 223 62 Lund, Sweden
[c]CEITEC – Central European Institute of Technology, Masaryk University, Kamenice 753/5, 625 00 Brno, Czech Republic

ARTICLE INFO

Keywords:
DivIVA protein
lipid membrane
molecular dynamics
negative curvature
lipid preference
N-terminal domain

ABSTRACT

DivIVA is a crucial membrane binding protein that helps to localize other proteins to negatively curved membranes at cellular poles and division septa in Gram-positive bacteria. The N-terminal domain of DivIVA is responsible for membrane binding. However, to which lipids the domain binds or how it recognizes the membrane negative curvature remains elusive. Using computer simulations, we demonstrate that the N-terminal domain of *Streptomyces coelicolor* DivIVA adsorbs to membranes with affinity and orientation dependent on the lipid composition. The domain interacts non-specifically with lipid phosphates via its arginine-rich tip and the strongest interaction is with cardiolipin. Moreover, we observed a specific attraction between a negatively charged side patch of the domain and ethanolamine lipids, which addition caused the change of the domain orientation from perpendicular to parallel alignment to the membrane plane. Similar but less electrostatically dependent behavior was observed for the N-terminal domain of *Bacillus subtilis*. The domain propensity for lipids which prefer negatively curved membranes could be a mechanism for the cellular localization of DivIVA protein.

1. Introduction

The correct localization of proteins in a cell is a crucial yet not well understood phenomenon. In Gram-positive bacteria, the conserved protein DivIVA acts as a cell polarity determinant and recruits other proteins to cell poles and cell division sites, thereby controlling important processes like cell division, chromosome localization, cell wall growth, and protein secretion [1, 2, 3, 4, 5, 6]. The targeting of DivIVA itself to cellular poles and division septa is not fully understood but involves an affinity for negatively curved membranes as a crucial localization factor [7, 8]. The ability of DivIVA to selectively target membrane regions with high negative curvature has been demonstrated by expression in heterologous organisms and in cells with genetically or artificially induced membrane distortions [7, 8, 9, 10, 11].

DivIVA protein is composed of a conserved N-terminal domain and a more variable C-terminal domain. The C-terminal domain forms a tetrameric coiled-coil, which drives oligomerization [12]. The N-terminal domain was shown to be responsible for membrane affinity [7, 8, 12]. Structural studies of DivIVA in *Bacillus subtilis* (Bsubt) has shown that the N-terminal domain forms a homodimer coiled-coil composed of two long parallel helices (residue 24-54) with two short helices (residue 2-10) attached to sides. Two loops between the short and long helices cross each other and form a domain tip, which was proposed to be important for the membrane interaction [12]. The loop was proposed to interact with the membrane via two phenylalanine residues inserted in the membrane and two arginine residues interacting with lipid head-groups. However, the molecular mechanisms of the curvature recognition and membrane interaction remains elusive.

Here we investigated the behavior of the N-terminal domain of DivIVA at membranes of different lipid composition including: phosphatidylcholine (POPC), phosphatidylethanolamine (POPE), phosphatidylglycerol (POPG), tetramyristoylcardiolipin with charge -1 e (TMCL1), and tetraoleylcardiolipin with charge -2 e (TOCL2). To evaluate the role of individual lipids we simulated model membranes composed of pure POPC, 1:1 mixtures of POPC-POPE and POPC-POPG, and tripartite mixture 11:5:4 POPC-POPG-TOCL2. In addition, we studied bacterial mimic membrane, 20:7:3 POPE-POPG-TMCL1, which composition is closer to bacterial membranes.

In particular, we were interested in the role of cardiolipin and ethanolamine lipids, which have intrinsic negative curvature [13, 14] and are enriched at cellular poles and division septa [15, 16] similarly to DivIVA [7, 8, 10]. ~~For~~We focus our study ~~we chose~~on DivIVA protein from *Streptomyces coelicolor* (Scoel), a homolog of DivIVA (Bsubt) for which high and low resolution structure of the N-terminal and C-terminal domain were determined, respectively [12]. DivIVA (Scoel) is interesting because it, in contrast to DivIVA (Bsubt), is essential for growth, orchestrates polar growth of the cell wall, and is instrumental in generating the new cell poles that lead to hyphal branching in streptomycetes [3, 17, 18]. It differs ~~also~~ from DivIVA (Bsubt) by having a leucine instead of the conserved phenylalanine residue at the tip of the N-terminal domain that was suggested to be important for interaction with membrane lipids [12]. Using all-atom molecular dynamics (MD) simulations we showed that the N-terminal domain of DivIVA Scoel interaction with membrane was mainly electrostatic and lipids with propensity to form negatively curved membranes played an important role. In contrast, Bsubt variant was less dependent on electrostatic interactions. Our findings confirm experimentally demon-

*Corresponding author
jurasek.m@gmail.com (M. Jurásek); robert.vacha@mail.muni.cz (R. Vácha)
ORCID(s):

strated affinity of the N-terminal domain towards lipid membranes and elucidate the interaction at atomic resolution.

2. Materials and Methods

All molecular dynamics (MD) simulations were performed in GROMACS 5.1.2 program package [19]. Two different parameterizations were employed: all-atom (AA) and coarse-grained (CG) models. All simulations were conducted at a temperature 309.15 K(AA) and 320 K (CG) in a 150 mM aqueous solution of NaCl at neutral pH. For details on system preparation and employed parameters of MD see Supplementary Material.

2.1. ~~Homology modelling~~Protein structures

Initial structure of the DivIVA N-terminal domain from *B. subtilis* (Bsubt) was based on its crystal model (PDB code 2WUJ) [12]. ~~We based our homology model of the DivIVA (Scoel) N-terminal domain on the crystal structure (PDB code 2WUJ) of a homolog domain from *B. subtilis* (Bsubt) [12].~~The structure of Bsubt homologue from *S. coelicolor* (Scoel) was derived by homology modeling from the Bsubt model. First 58 residues of DivIVA (Scoel) have ≈ 48% sequence identity and ≈ 65% sequence similarity with its 52 residue long template, see Fig. 1a. Even though the sequence identity is not particularly high, the surface electrostatic pattern is conserved (see Fig. 1b) with the positively charged domain tip and negatively charged sides. The charge pattern is more pronounced in DivIVA (Scoel), where the negatively charged patch is larger compared to DivIVA (Bsubt). The sequence of the membrane interacting loop changes from SFR motif to RLR [4] in Scoel which might cause the interaction to be electrostatic rather than hydrophobic. The homology model was constructed with the Swiss-Model [20], from which the best structure was selected as an initial structure for MD equilibration. The ~~model~~ stability ~~was~~of homology model and the original Bsubt structure were tested in 100 ns long all-atom MD simulations. Root mean squared deviations (RMSDs) of ~~protein backbone~~the N-terminal domains converged in the first 5 ns of the simulation. Afterwards structure fluctuated within the RMSD range of 0.15 nm (see Fig. S1).

2.2. Domain orientation

To quantify the domain orientation preference we defined three orthogonal vectors within the domain and measured their angle with respect to the membrane normal. The first vector, which is defined between C_α atoms of Arg 19 in Scoel (Phe 17 in Bsubt) of both chains and the center of mass of Leu 52 in Scoel (Leu 46 in Bsubt) , represents the domain long axis and its angle from the membrane normal is denoted as α. The second vector connects N atom of Val 8 (Ile 8 in Bsubt) from both chains and the angle between the vector and the membrane normal is denoted as β. The third vector connects N atom of Val 34 in Scoel (Val 32 in Bsubt) from both chains and the angle between the vector and the membrane normal is denoted as γ. The angle α describes how much is the domain tilted to the membrane, while angles γ and β show preference of the long or the short helix to point to the membrane.

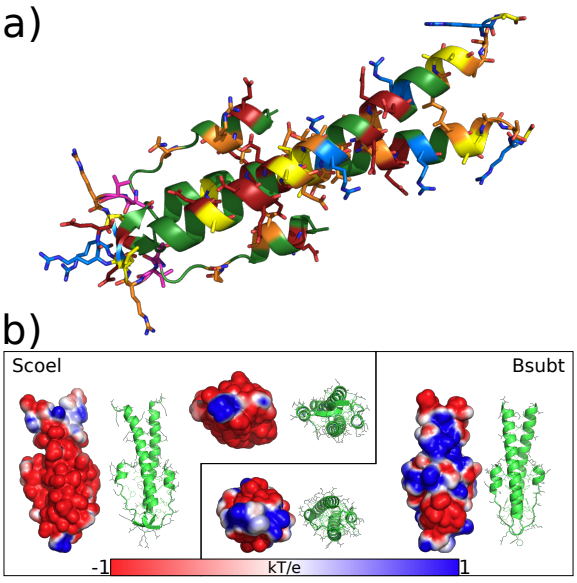

Figure 1: Comparison between the N-terminal domain of DivIVA protein from *S. coelicolor* (Scoel) and *B. subtilis* (Bsubt). a) Homology model of DivIVA (Scoel) (residue 2-58) with residues colored based on the sequence comparison with the template of DivIVA (Bsubt). Conserved residues are shown in green, mutations keeping the residue character are displayed in orange, sequence extensions are colored in purple, mutations exchanging polar or charged residues to hydrophobic are shown in yellow, and mutations which introduced charge instead of polar or hydrophobic residues or changed charge of the residue are displayed in red and blue when changed to negative and positive charge, respectively. b) Electrostatic potential at the protein surface calculated with APBS [21] plug-in [22] in PyMOL [23] considering 150 mM monovalent salt at 310K.

2.3. Membrane-domain interaction

~~To calculate the mean enthalpic contribution of different lipid and protein moieties to overall membrane-protein interaction we divided lipids and protein into few groups.~~We divided lipids and protein into few groups to calculate the mean enthalpic contribution of different lipid and protein moieties to overall membrane-protein interaction. Protein was divided into five groups, one group for each charged residue (aspartic acid, glutamic acid, lysine, and arginine) and one group for all uncharged residues. Lipids were divided into four moieties: lipid tails, glycerol, phosphate, and rest of the headgroup moiety (choline, ethanolamine or head-group glycerol).

3. Results

3.1. The Scoel N-terminal domain adsorption

The N-terminal domain was found to adsorb to all tested membranes at least in one of the independent simulation trajectories. The final configurations of all simulated systems are grouped based on the membrane composition and ~~are~~ depicted in Fig. 2.

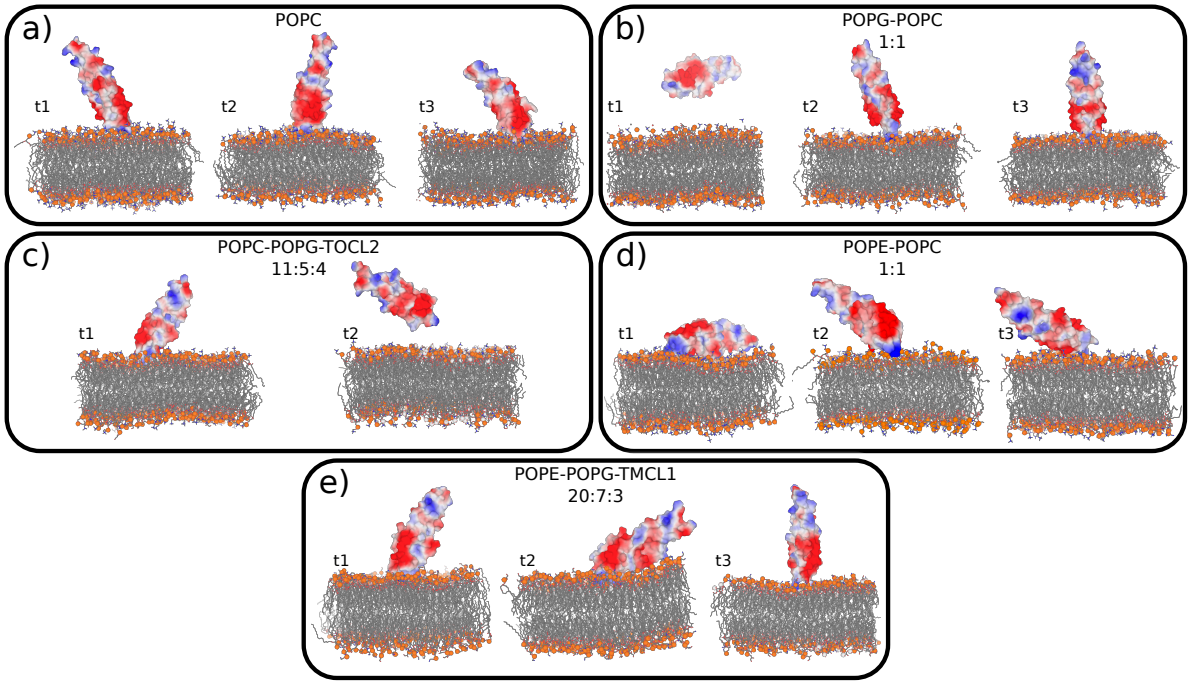

Figure 2: The simulation snapshots ~~from all simulations~~ depicting the Scoel N-terminal domain adsorption/desorption at membranes of various lipid compositions. Each item a-e) contains snapshots taken at the end of each independent ~~simulation~~ trajector~~ies~~y labeled t1-t3. In case of 1:1 POPG-POPC t1 and 11:5:4 POPC-POPG-TOCL2 t2, snapshots were taken when the protein desorbed. The N-terminal domain dimer is shown with water accessible surface ~~model~~ colored ~~red and blue for negative and positive charge, respectively.~~based on the charge density. Red and blue colors stand for negative and positive charge, respectively. The membrane is displayed with stick model where aliphatic tails are colored in gray and the rest of the lipid is colored base on the atom (red O, blue N, orange P). Solvent and hydrogen atoms of lipids are omitted for clarity.

In case of a POPC membrane with zero net charge, we did not observe desorption in any of three simulations. The positively charged domain tip was integrated into the lipid head-group region (see Fig. 2), while the rest of the domain remained in a solution. Similarly in the both anionic-lipid containing 1:1 POPG:POPC and 11:5:4 POPC-POPG-TOCL2 membranes, the N-terminal domain interacted only via its tip. Interestingly, in both membranes with POPG, we observed the domain desorption in one of the simulations. The desorption in 1:1 POPG-POPC membrane occurred after $\approx$ 40 ns and domain did not readsorb to the membrane within the next 60 ns (see Fig. S2 a). In the simulation trajectory t2 of 11:5:4 POPC-POPG-TOCL2 membrane, we observed a series of desorption and adsorption events. The first desorption occurred relatively fast within the first $\approx$ 15 ns followed by the domain resorption to another leaflet of the membrane at $\approx$ 30 ns where it remained adsorbed for $\approx$ 90 ns (see Fig. S2 a). During all the above simulations, the domain remained adsorbed only with shallow insertion of the domain tip in the membrane. To inspect binding contribution of different lipid and protein moieties, we calculated the individual enthalpic contributions to the protein-membrane interaction (see Fig. 3). We found that the contribution from lipid tails was negligible for all systems and majority of the interactions was between the domain and lipid head-groups. Particularly prominent was interaction between lipid phosphates and arginine residues at the tip, Arg 17 and Arg 19, present in all studied systems. In pure POPC, 1:1 POPG-POPC, and 11:5:4 POPC-POPG-TOCL2 this interaction was responsible for adsorption, i.e. there was no other significant interaction between the domain and membranes. Note that the interaction was especially strong with cardiolipin in single depronated state (TMCL1) in 20:7:3 POPE-POPG-TMCL1 membrane which is a mimic of bacterial membrane without POPC [24]. In this membrane, cardiolipin interacted with both its phosphate groups with the arginines (see Fig. 3 e).

Very distinct behavior of the domain was found in the membranes containing POPE lipids. In the 1:1 POPE-POPC membrane, the domain remained adsorbed in all three simulations, where we found additional domain-lipid interaction. The additional interaction was mediated by negatively charged acidic residues (Glu and Asp) on the domain and ethanolamine head-groups from POPE lipids (see Fig. 3 d-e). The phosphate interactions with the tip arginines were still present, however, glutamic and aspartic acids interactions dominated the overall domain-membrane enthalpy. Note that even though the interaction strength per one amino-acid might be smaller than that of arginines the number of glutamic and aspartic acids' contacts resulted in a strong interaction with the membrane. Additionally, the second set of arginine residues (Arg 9, Arg 43, and Arg 57 in DivIVA (Scoel)), located on the opposite end of the domain than the tip, interacted with same strength as tip arginines with the membrane in 1:1 POPE-POPC t1 (see Fig. S6). ~~resulting~~Interaction

of POPE lipids with acidic residues at the domain side resulted in the parallel alignment of the domain to the membrane plane. Similar ~~behavior~~parallel alignment was found in the second simulation trajectory, t2, of 20:7:3 POPE-POPG-TMCL1 membrane, where the domain was strongly tilted toward the membrane surface. ~~However, such tilt was found only in two out of six simulations containing POPE lipids in the timescale of our simulations.~~To study the concentration independent effect of POPE lipids, we also simulated pure POPE membrane. As expected, the effect of POPE was much stronger and the domain adopted parallel alignment within 30 ns (see Fig. S7). Note that parallel orientation of the domain was observed only three times out of seven simulations of membranes containing POPE lipids (including pure POPE membrane). This might be caused by limited timescale of our simulations.

3.2. The Scoel N-terminal domain orientation on the membrane

We observed a range of possible orientations of the adsorbed N-terminal domain in the range from perpendicular to parallel orientation to the membrane plane. To analyze the orientations in detail we defined three orthogonal vectors within the domain. The angles of those vectors from the membrane normal capture the domain orientation (see scheme in the middle of Fig. 4 and the Methods section). In brief, the angle α determines the orientation of the main axis of the domain. The parallel or perpendicular orientation to the membrane plane leads to the $\cos(\alpha)$ being 0 or 1, respectively. The angles β and γ describe the orientation of the long and short helix toward the membrane. For example, if the domain is tilted to the membrane with the short helix pointing to the membrane we get $\cos(\beta)$ close to 1.

The probability distributions of the domain orientations with respect to the membrane are shown in Fig. 4. In pure POPC membrane, the domain was mostly perpendicular to the membrane with maximum tilt up to $\cos(\alpha) \approx 0.5$. In the t1 and t3 simulation trajectories of POPC, we did not observe any preference to orient neither the long nor the short helix toward the membrane, i.e. there is no significant difference between distributions of γ and β for tilted domain (~~$\cos\alpha < 1$~~$\cos(\alpha) < 1$). In case of t2, there is a slight preference of the domain to orient with long helix to the membrane, i.e. $\cos(\gamma)$ increases with increasing tilt while $\cos(\beta)$ remains low. Slightly stronger preference for perpendicular orientation could be found in 1:1 POPG-POPC membrane. All probability maxima were present in close proximity of bottom-right corner of the plot which corresponds to the perpendicular orientation of the domain (see Fig. 4 b). Reduced resolution of probability distribution in the t1 simulation trajectory of 1:1 POPG-POPC is due to the domain desorption leading to a shorter sampling of adsorbed state. Perpendicular orientation was also preferred in 11:5:4 POPC-POPG-TOCL2 membrane similarly to pure POPC and 1:1 POPG-POPC (see Fig. 4 c). Slightly higher preference of the short helix to point to the membrane could be found in the simulation trajectory t1, where the $\cos(\beta)$ reached higher values for lower $\cos(\alpha)$. Large tilt freedom in simulation trajectory t2 is due to configurations sampled just before desorption.

In contrast to the membranes mentioned above, a distinct behavior of the domain was observed in the presence of POPE lipids. On 1:1 POPE-POPC membranes, the domain also preferred high tilt (t2 and t3) or even parallel orientations (t1) to the membrane with long helix pointing to the membrane (see lower $\cos(\alpha)$ in Fig. 4 d). The origin of this preference is in the interaction between POPE lipids and negatively charged patch situated at the long helix (see Fig. 3 d-e). The amount of negative residues interacting with POPE determined the tilt of the domain which differ in various simulation trajectories t1-3. In case of 20:7:3 POPE-POPG-TMCL1 membranes, the domain was tilted in t2 simulation trajectory, while the domain remained perpendicular to the membrane in t1 and t3 simulations. We observed strong preference of the short helix toward the membrane in simulation trajectory t2. However, in other two simulation trajectories (t1 and t3) the domain rather preferred facing the membrane with the long helix during the domain tilting ($\cos(\gamma)$ increased with decreasing $\cos(\alpha)$). The long helix was also pointing to a membrane in pure POPE membrane (see Fig. S7 c).

Note that, when the domain was adsorbed at the membrane in a parallel orientation, the domain induced a slight negative curvature on the membrane, which followed the domain convex shape (see Fig. 2 d t1 and e t2).

3.3. Distribution of specific lipids around the Scoel N-terminal domain

The lipid composition was found to be important for the domain adsorption and its orientation preference, which demonstrated a specific role of POPE lipids. Therefore, we analyzed the distribution of different lipids around the domain (see Fig. 5).

POPE lipids were found to cluster in the vicinity of the negatively charged domain patch with occasional presence of POPC in 1:1 POPE-POPC membrane. Even stronger POPE clustering was found in case of 20:7:3 POPE-POPG-TMCL1 membrane, where a large continuous cluster of POPE lipids was situated at the contact with the negatively charged patch (see Fig. 5). The increased density of POPE head-groups below the negatively charged patch was also observed in pure POPE membrane (see Fig. S7 d).

In contrast, negatively charged lipids, POPG and TMCL1 ~~at~~in POPE-POPG-TMCL1 membrane, accumulated at the domain tip and C-end, where are arginine-rich clusters. Clusters of negatively charged lipids in a close proximity to the domain tip were also found in both negatively charged membranes without POPE (1:1 POPG-POPC and 11:5:4 POPC-POPG-TOCL2, see Fig. 5 b-c). These clusters were surrounded by POPC lipids especially in the direction of negatively charged patches of the domain probably due to the local electrostatic depletion of negatively charged lipids. In case of the pure POPC lipid membrane, we observed only slightly increased density of POPC in the proximity of arginine-rich domain tip (see Fig. 5 a).

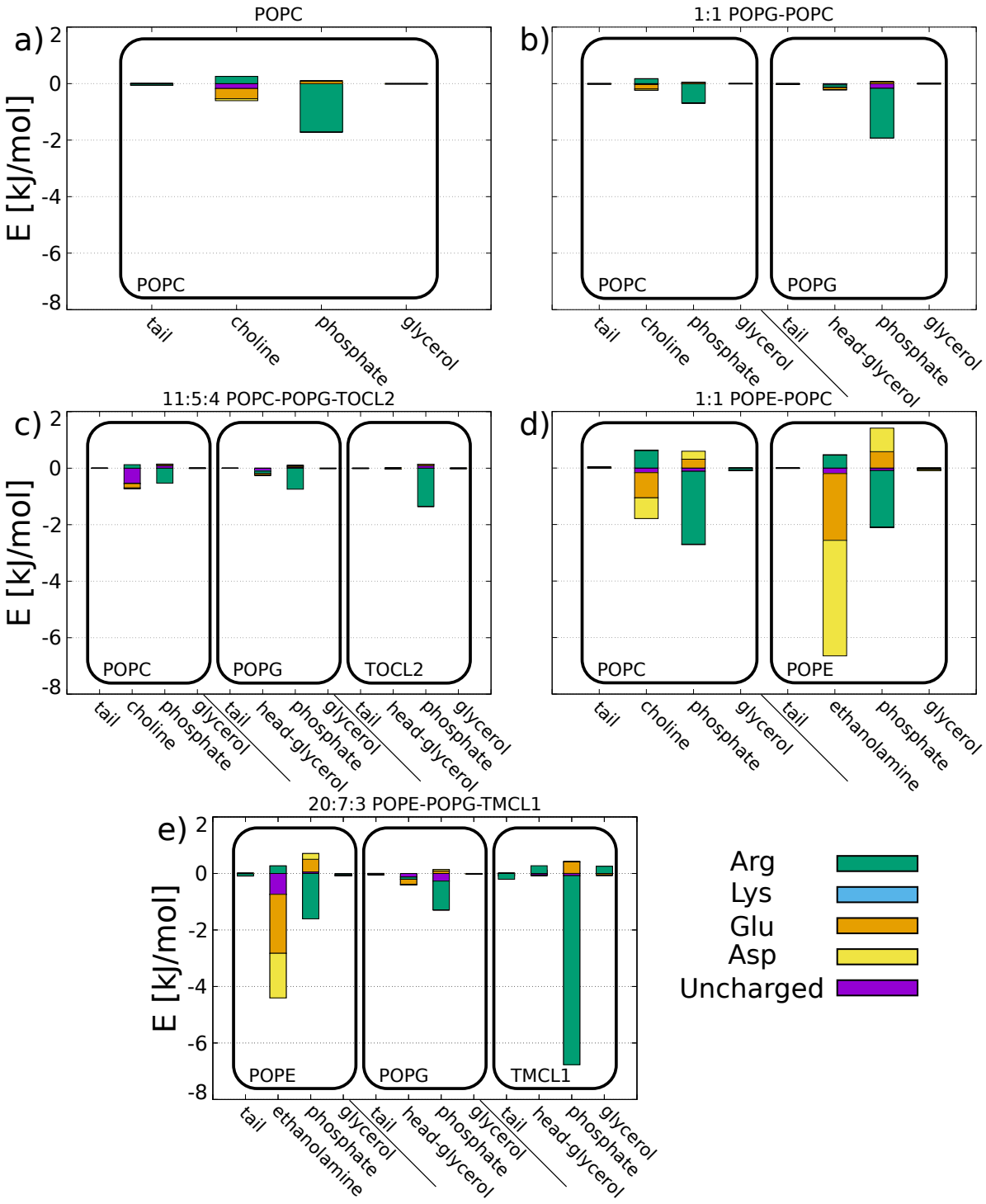

Figure 3: Average interaction strength per one lipid between the membrane and the Scoel N-terminal domain averaged over all independent simulations. Contributions were split into specific lipids parts and protein charged residues. Each lipid is divided into four ~~parts~~moieties: tail, glycerol, phosphate, and head-group~~moiety~~. Interaction of the each lipid moiety with different charged and uncharged residues are ~~depicted via~~coloured differently ~~colours~~ (see legend). Parts of each lipid are grouped together in rectangles for clarity.

3.4. Comparison to the ~~*Bacillus subtilis*~~Bsubt N-terminal domain

For comparison, we also simulated the interaction between membranes and the Bsubt N-terminal domain. We tested two membrane compositions, which had the strongest effects on the Scoel N-terminal domain: pure POPE and 1:1 POPG-POPC. Each membrane was studied with two independent simulations.

In all simulations, the domain from Bsubt remained bound to the membrane with its tip buried within and below lipid

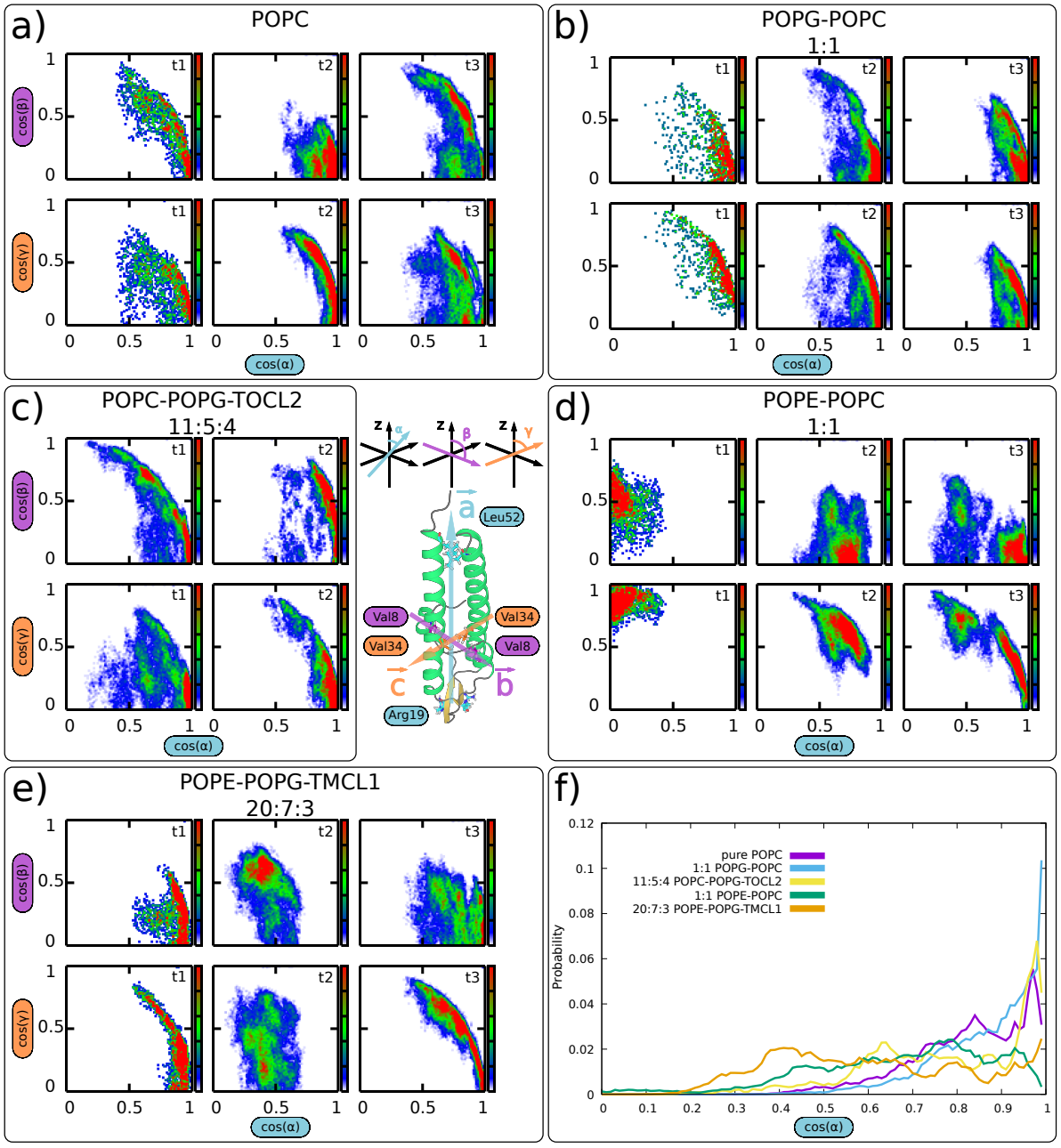

Figure 4: The Scoel N-terminal domain orientation on membranes with different lipid composition. In the middle, vectors describing the N-terminal domain orientation are displayed. Vector $\vec{a}$ is defined between the center of mass of Leu 52 and the C_α atoms of Arg 19. Vector $\vec{b}$ and $\vec{c}$ are defined by the N atoms of Val 8 and Val 34 from both chains, respectively. Angles α, β, and γ are angles between membrane normal (Z-axis) and vectors $\vec{a}$, $\vec{b}$, and $\vec{c}$, respectively. a-e) probability distributions of different domain orientations from all simulated membranes. Data were collected over the last 100 ns of simulations. The orientations of desorbed domain are excluded. Simulation trajectory indexes (t1, t2, t3) are shown in the top-right ~~part~~corner of each 2D probability distribution. Color coding of probabilities is white, blue, green, and red for intervals (0-0.0001), (0.0001-0.0005), (0.0005-0.001), and (0.001-1), respectively. f) Probability distribution of cos(α) for each membrane composition, where perpendicular orientation corresponds to 1, while tilted orientations correspond to lower values of cos(α).

head-groups, where two Phe 17 residues at the tip interacted with lipid tails (see Fig. S2 b). Such binding is different from the Scoel N-terminal domain, which interacted mainly with lipid phosphates and desorbed from negatively charged membranes (1:1 POPG-POPC t2 and 11:5:4 POPC-POPG-TOCL2 t2). The orientations of the domains were similar for both DivIVA variants with perpendicular orientation on 1:1 POPG-POPC membrane and tilted orientation on membranes with POPE (see Fig. 6). However, the preference for a tilted orientation at POPE membranes was much weaker and parallel orientation was not achieved with the domain from Bsubt.

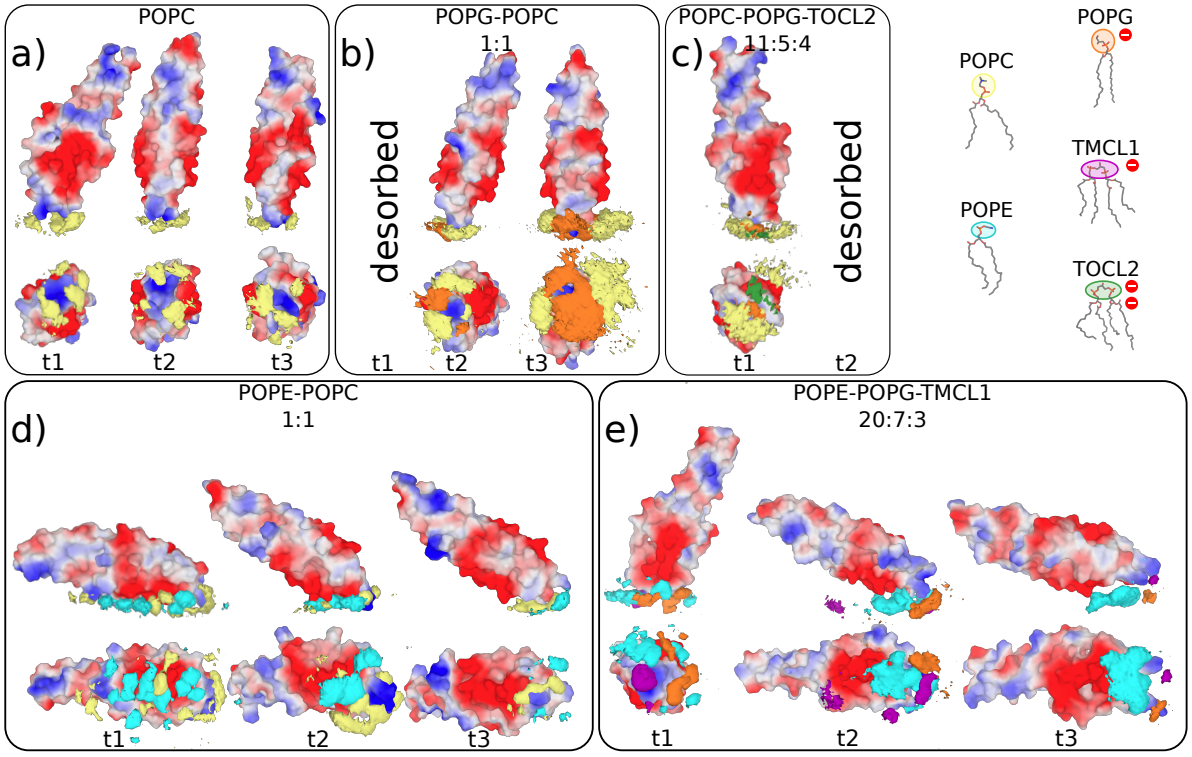

Figure 5: Averaged number density of lipid head-groups around the N-terminal domain of DivIVA (Scoel) at membranes with different lipid compositions. For each simulation, side and bottom views from the membrane are shown in the top and bottom snapshots, respectively. High density of each head-group is depicted with isosurface colored based on the lipid type (POPC yellow, POPE cyan, POPG orange, TMCL1 purple, and TOCL2 is green). Color legend and structure of each lipid are shown in the top right corner. The N-terminal domain is depicted with vdW surface colored based on the surface charge density with red and blue colors corresponding to negative and positive charge, respectively. Simulations with the desorbed domain from the membrane are not shown.

The lipid distribution was similar for both domain variants. The POPG head-groups were enhanced in the vicinity of the positively charged tip with POPC slightly enhanced in the proximity of negatively charged patches on 1:1 POPG-POPC membrane. The depletion of POPG lipids from the vicinity of the negatively charged patch was weaker in case of the Bsubt. In the pure POPE membrane, we can see a slight increase in the density of POPE head-groups around the Bsubt domain tip.

3.5. Comparison of Martini and all-atom simulations

To study the Scoel domain adsorption at longer time scales and with larger system sizes we employed Martini coarse-grained force-field [25, 26, 27]. We performed two types of simulations where the N-terminal domain fold was either fixed with elastic bonds or not fixed (see the Methods section). Despite the domain stable fold in solution, without elastic bonds the domain unfolded at the membrane and partially inserted the short α-helix among lipids (see Fig. S3–S5). Because we have not observed similar unfolding in all-atom simulations and it is recommended to keep the fold with elastic bonds, the unfolding is likely an artifact. The restrained domain with elastic bond remained stable as in the all-atom simulations, but the affinity to membranes was different. The domain adsorbed only to membranes with cardiolipin (11:5:4 POPC-POPG-CL2, and 20:7:3 POPE-POPG-CDL1). Membranes without cardiolipin (pure POPC, 1:1 POPE-POPC, and 1:1 POPG-POPC) were not able to keep the domain adsorbed even after 1 μs long equilibration, during which the domain was held in close proximity to the membrane.

4. Discussion

We studied membrane binding of DivIVA protein from *S. coelicolor*(Scoel), which recognizes cell poles and presumably negatively curved membranes as does its homologue from *B. subtilis*(Bsubt). In particular, the behavior of the N-terminal domain homodimer was investigated at six different membrane compositions: pure POPC ~~,~~and POPE and mixtures 1:1 POPG-POPC, 11:5:4 POPC-POPG-TOCL2, 1:1 POPE-POPC, and 20:7:3 POPE-POPG-TMCL1. The N-terminal domain adsorbed to all tested membrane compositions, but its affinity and preferred orientation on the membrane was dependent on ~~its~~the lipid composition.

Starting from general features, the domain from Scoel interacted with all membranes with four arginines and two leucines at the domain tip. The arginines formed salt-bridges with lipid phosphates, particularly strong with cardiolipin.

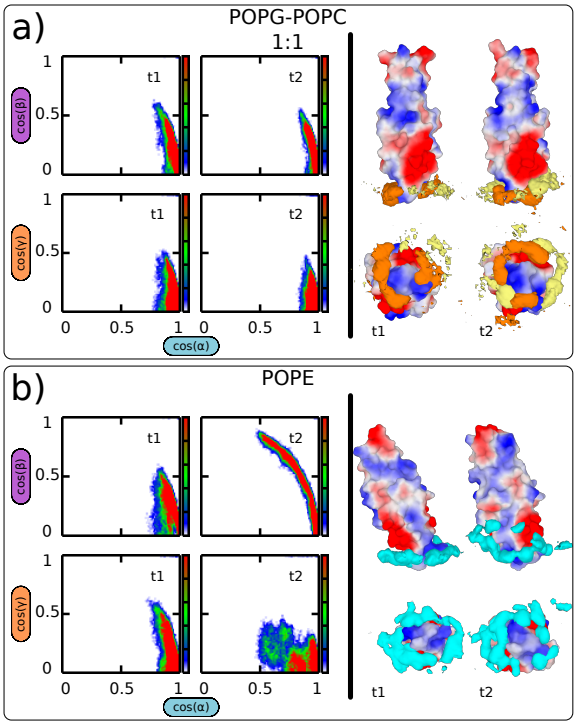

Figure 6: Interaction of the Bsubt N-terminal domain with a) 1:1 POPG-POPC and b) pure POPE membrane. Each panel show orientation of the domain with respect to the membrane and the density of lipids in the vicinity of the domain tip in the left and right section, respectively. Angles are calculated similarly to Fig. 4. Vector $\vec{a}$ is defined between the center of mass of Leu 46 and the C_α atoms of Phe 17. Vector $\vec{b}$ and $\vec{c}$ are defined by the N atoms of Ile 8 and Val 32 from both chains, respectively. For color coding of lipids in density maps see Fig. 4.

This might be due to unusual arrangement of two phosphate groups in cardiolipin that are available for interaction with arginine. Note that phosphate-arginine interaction is known to be exceptionally strong [28] and cardiolipin content in Scoel membranes is high being 30% or higher [29, 30]. Without any additional interaction the domain preferred perpendicular orientation to the membrane plane. This mode of adsorption seems to be responsible for the general affinity of the Scoel's DivIVA protein to the bacterial membranes. Note that the domain tip amphiphilicity and positive charge are similar to antimicrobial peptides which target bacterial membranes. However, the domain-membrane interaction was not strong enough to overcome electrostatic repulsion with the ~~negaitively~~negatively charged domain patch at membranes with negatively charged lipids (1:1 POPG-POPC, 11:5:4 POPC-POPG-TOCL2), where the domain occasionally desorbed. Thus electrostatic interaction seems to play a major role in Scoel's DivIVA affinity towards membranes suggesting possible interaction dependence on local pH and salt concentration.

In presence of POPE lipids, the domain additionally interacted with ethanolamine groups on POPE via a negatively charged patch on the domain side. This interaction caused the domain to tilt to the membrane, which resulted in the full parallel orientation of the domain to the membrane in ~~two~~some of the systems with Scoel's DivIVA. In such cases, the membrane adopted slightly negatively curved topology following the domain convex shape in the direction of the long helix. DivIVA has previously not been reported to impose curvature on membranes, but it should be noted that DivIVA (Scoel) in the cell is observed to localize into clusters along the lateral cell wall. These clusters appear to trigger the formation of new cell poles, which is a process that involves the imposition of negative curvature on the cytoplasmic membrane. [17] Thus, it is possible that DivIVA (Scoel) could contribute to this process by facilitating the bending of membranes contrary to DivIVA (Bsubt) which is not known to have such priming role.

POPE lipids, which have slightly negative intrinsic curvature, clustered below the patch. The additional interaction of the domain with POPE lipids could thus be responsible for the localization of DivIVA proteins to membranes with increased POPE content. Indeed, POPE and DivIVA are known to concentrate at highly curved surfaces such as membranes at cell poles or division septa. [31] Moreover, cardiolipin, which has also preference for negatively curved membranes, was interacting with the domain tip the strongest and thus could further strengthen the protein localization. Therefore, our results suggest that lipid-specific interactions of ~~Scoel~~ DivIVA could contribute to its affinity for cell poles and other regions with negatively curved membranes.

Despite the high degree of homology between the N-terminal domain of DivIVA from ~~*S. coelicolor*~~Scoel and ~~*B. subtilis*~~ (Bsubt~~)~~, there are important differences in the ~~regions interacting~~interactic with membrane. The tip contains two arginine, two serine, and two phenylalanine residues in Bsubt compared to four arginine and two leucine residues in Scoel. The replacement of arginine by serine residues in Bsubt is expected to weaken the general electrostatic interaction with membrane. In contrast, the change of leucine to phenylalanine residues in Bsubt strengthen the hydrophobic interaction with lipids. ~~To complicate the transferability of our results to other DivIVA protein further, the size of negatively charged side patch is reduced to half in Bsubt compared to Scoel. Therefore, either the POPE-Asp/Glu interactions and the related induced domain tilt is specific in Scoel or these interactions are substituted by other residues and lipids in Bsubt.~~ Indeed, the simulated Bsubt variant had the domain tip buried deeper in the membrane compared to the Scoel variant. Therefore, the Bsubt N-terminal domain is expected to be more sensitive to the saturation of lipid tails. Moreover, the negatively charged side patch is smaller on the Bsubt N-terminal domain, which further modifies its electrostatic interactions and reduces preference for POPE lipids. Indeed, no unbinding events from the negatively charged membrane were observed for the Bsubt domain and its tilt on the POPE membrane was smaller compared to the Scoel variant.

The observed changes in the ~~domain~~N-terminal domain orientation at the membrane could affect the domain binding to its interaction partners. The availability and expo-

sure of the negatively charged patches on the domain seems to be crucial, because MinJ membrane protein is known to bind ~~close to the negative patch on the domain~~in the vicinity of the negatively charged patch [32]. Moreover, a negatively charged patch on the N-terminal domain of GpsB, a homolog to the N-terminal domain of DivIVA, has already been identified as a key protein binding site [33]. When the N-terminal domain of DivIVA is adsorbed on a membrane in the perpendicular orientation, both its negative patches are available. In contrast, during the parallel adsorption one of the patches is interacting with the membrane, while the second patch is exposed to the solution. Note that the change in the orientation of the N-terminal domain is not expected to interfere with the C-termini oligomerization in Scoel due to a roughly 130 residues long linker connecting the domains. In contrast, the linker is only several residues long in the Bsubt DivIVA, thus change in the N-terminal orientation at a membrane could interfere with the DivIVA oligomerization. ~~This~~Our findings suggest an intricate relation between the domain binding mode and accessibility of the domain surface for its binding partners.

Note that lipids were able to diffuse on average 2 nm during the time scale of our simulation, therefore the size of the POPE patch below the domain and the extent of the domain tilt could be affected by the length of our simulations with multi-component membranes. The limited sampling also prevented us from the calculation of the membrane induced negative curvature. In order to enhance the sampling we carried out simulations with coarse-grained Martini model [25, 26, 27]. Unfortunately, these simulations were not able to reproduce the all-atom behavior and the domain desorbed from all membranes without cardiolipin. This is likely to be an imperfection of the coarse-grained model, in which the electrostatics is rather short ranged and the atomistic shape of a molecule is simplified [26, 34].

5. Conclusions

~~In rod-shaped or filamentous bacterial cells, a spatial organization of proteins is largely dependent on the proper recognition of cellular poles, which is usually mediated by landmark proteins, such as DivIVA [1, 2, 3, 4, 5]. DivIVA was shown to have an intrinsic affinity towards negatively curved membranes [7, 8, 9, 10, 11] and to serve as a guide for other proteins adsorbing to polar ends of the cell [1, 2, 3, 4, 5]. However, means by which DivIVA adsorb to the membrane and recognize negative curvature remains unknown.~~We investigated the interaction between membranes of different lipid compositions and DivIVA proteins, which were shown to have an intrinsic affinity to negatively curved membranes [7, 8, 9, 10, 11] and guide other proteins to polar ends of the cell. [1, 2, 3, 4, 5] However, means by which DivIVA adsorb to the membrane and recognize negative curvature remains unknown.

We investigated the interaction of the N-terminal domain of DivIVA from *S. coelicolor* (Scoel) with membranes of different lipid composition. Using molecular dynamics simulations, we found that the N-terminal domain adsorbs unspecificaly to all membranes ~~via~~with its tip. The tip interacted via arginine residues with lipid phosphates, especially with those from cardiolipin. Upon addition of POPE lipids we observed a change in the domain orientation from perpendicular to tilted or even parallel to the membrane plane. This arrangement was stabilized by the negatively charged residues on the domain side interacting with partially positively charged amines in POPE head-groups, which created a cluster below the domain. The observed behavior was different for the N-terminal domain from *B. subtilis* which binding to membranes was less electrostatically driven and resulted in stronger preference for perpendicular orientation than the domain from Scoel.

~~Such~~The observed lipid specific interaction could rationalize the membrane localization of DivIVA and can regulate binding of other proteins to the domain. Moreover, because the domain-membrane interaction is dominated by electrostatics in Scoel, we expect the interaction to be influenced by the properties of surrounding environment such as pH or salt concentration.

Acknowledgement

This work was supported by the Czech Science Foundation (grant 17-11571S to R.V.), Grant Agency of Masaryk University (MUNI/G/ 1100/2016), and the CEITEC 2020 (LQ1601) project with financial contribution made by the Ministry of Education, Youths and Sports of the Czech Republic within special support paid from the National Programme for Sustainability II funds. K.F. is supported by grant from Swedish Research Council (2015-05452). Computational resources were provided by the CESNET LM2015042 and the CERIT Scientific Cloud LM2015085, provided under the programme 'Projects of Large Research, Development, and Innovations Infrastructures'. This work was supported by The Ministry of Education, Youth and Sports from the Large Infrastructures for Research, Experimental Development and Innovations project 'IT4Innovations National Supercomputing Center – LM2015070'.

Competing interests

The authors declare that they have no conflict of interest.

Transparency document

The Transparency document associated with this article can be found in the online version.

Appendix A. Supplementary data

Supplementary data to this article can be found online at doi: XXX.

References

[1] S. Ben-Yehuda, D. Z. Rudner, R. Losick, RacA, a bacterial protein that anchors chromosomes to the cell poles, Science 299 (2003) 532–536.

[2] M. Bramkamp, R. Emmins, L. Weston, C. Donovan, R. A. Daniel, J. Errington, A novel component of the division-site selection system of *Bacillus subtilis* and a new mode of action for the division inhibitor MinCD, Molecular microbiology 70 (2008) 1556–1569.

[3] K. Flärdh, Essential role of DivIVA in polar growth and morphogenesis in *Streptomyces coelicolor* A3 (2), Molecular microbiology 49 (2003) 1523–1536.

[4] S. Halbedel, R. J. Lewis, Structural basis for interaction of DivIVA/GpsB proteins with their ligands, Molecular microbiology 111 (2019) 1404–1415.

[5] B. Sieger, M. Bramkamp, Interaction sites of DivIVA and RodA from *Corynebacterium glutamicum*, Frontiers in microbiology 5 (2015) 738.

[6] L. R. Hammond, M. L. White, P. J. Eswara, ¡ vIVA la DivIVA!, Journal of bacteriology (2019) JB–00245.

[7] R. Lenarcic, S. Halbedel, L. Visser, M. Shaw, L. J. Wu, J. Errington, D. Marenduzzo, L. W. Hamoen, Localisation of DivIVA by targeting to negatively curved membranes, The EMBO journal 28 (2009) 2272–2282.

[8] K. S. Ramamurthi, R. Losick, Negative membrane curvature as a cue for subcellular localization of a bacterial protein, Proceedings of the National Academy of Sciences 106 (2009) 13541–13545.

[9] L. D. Renner, P. Eswaramoorthy, K. S. Ramamurthi, D. B. Weibel, Studying biomolecule localization by engineering bacterial cell wall curvature, PloS one 8 (2013) e84143.

[10] D. H. Edwards, H. B. Thomaides, J. Errington, Promiscuous targeting of *Bacillus subtilis* cell division protein DivIVA to division sites in *Escherichia coli* and fission yeast, The EMBO journal 19 (2000) 2719–2727.

[11] J. Pogliano, N. Pogliano, J. A. Silverman, Daptomycin-mediated reorganization of membrane architecture causes mislocalization of essential cell division proteins, Journal of bacteriology 194 (2012) 4494–4504.

[12] M. A. Oliva, S. Halbedel, S. M. Freund, P. Dutow, T. A. Leonard, D. B. Veprintsev, L. W. Hamoen, J. Löwe, Features critical for membrane binding revealed by DivIVA crystal structure, The EMBO journal 29 (2010) 1988–2001.

[13] B. Kollmitzer, P. Heftberger, M. Rappolt, G. Pabst, Monolayer spontaneous curvature of raft-forming membrane lipids, Soft matter 9 (2013) 10877–10884.

[14] E. Beltrán-Heredia, F.-C. Tsai, S. Salinas-Almaguer, F. J. Cao, P. Bassereau, F. Monroy, Membrane curvature induces cardiolipin sorting, Communications Biology 2 (2019) 225.

[15] E. Mileykovskaya, W. Dowhan, Visualization of phospholipid domains in Escherichia coli by using the cardiolipin-specific fluorescent dye 10-N-nonyl acridine orange, Journal of bacteriology 182 (2000) 1172–1175.

[16] L. D. Renner, D. B. Weibel, Cardiolipin microdomains localize to negatively curved regions of *Escherichia coli* membranes, Proceedings of the National Academy of Sciences 108 (2011) 6264–6269.

[17] A. M. Hempel, S.-b. Wang, M. Letek, J. A. Gil, K. Flärdh, Assemblies of DivIVA mark sites for hyphal branching and can establish new zones of cell wall growth in *Streptomyces coelicolor*, Journal of bacteriology 190 (2008) 7579–7583.

[18] D. M. Richards, A. M. Hempel, K. Flärdh, M. J. Buttner, M. Howard, Mechanistic basis of branch-site selection in filamentous bacteria, PLoS computational biology 8 (2012) e1002423.

[19] M. J. Abraham, T. Murtola, R. Schulz, S. Páll, J. C. Smith, B. Hess, E. Lindahl, GROMACS: high performance molecular simulations through multi-level parallelism from laptops to supercomputers, SoftwareX 1 (2015) 19–25.

[20] M. Biasini, S. Bienert, A. Waterhouse, K. Arnold, G. Studer, T. Schmidt, F. Kiefer, T. G. Cassarino, M. Bertoni, L. Bordoli, T. Schwede, SWISS-MODEL: modelling protein tertiary and quaternary structure using evolutionary information, Nucleic acids research 42 (2014) W252–W258.

[21] N. A. Baker, D. Sept, S. Joseph, M. J. Holst, J. A. McCammon, Electrostatics of nanosystems: application to microtubules and the ribosome, Proceedings of the National Academy of Sciences 98 (2001) 10037–10041.

[22] M. Lerner, H. Carlson, APBS plugin for PyMOL, Ann Arbor: University of Michigan (2006).

[23] Schrödinger, LLC, The PyMOL molecular graphics system, version 1.8, 2015.

[24] C. Sohlenkamp, O. Geiger, Bacterial membrane lipids: diversity in structures and pathways, FEMS microbiology reviews 40 (2016) 133–159.

[25] S. J. Marrink, A. H. De Vries, A. E. Mark, Coarse grained model for semiquantitative lipid simulations, The Journal of Physical Chemistry B 108 (2004) 750–760.

[26] S. J. Marrink, H. J. Risselada, S. Yefimov, D. P. Tieleman, A. H. De Vries, The MARTINI force field: coarse grained model for biomolecular simulations, The journal of physical chemistry B 111 (2007) 7812–7824.

[27] L. Monticelli, S. K. Kandasamy, X. Periole, R. G. Larson, D. P. Tieleman, S.-J. Marrink, The MARTINI coarse-grained force field: extension to proteins, Journal of chemical theory and computation 4 (2008) 819–834.

[28] A. S. Woods, S. Ferré, Amazing stability of the arginine-phosphate electrostatic interaction, Journal of proteome research 4 (2005) 1397–1402.

[29] M. Sandoval-Calderón, O. Geiger, Z. Guan, F. Barona-Gómez, C. Sohlenkamp, A eukaryote-like cardiolipin synthase is present in *Streptomyces coelicolor* and in most actinobacteria, Journal of Biological Chemistry 284 (2009) 17383–17390.

[30] M. Sandoval-Calderón, D. D. Nguyen, C. A. Kapono, P. Herron, P. C. Dorrestein, C. Sohlenkamp, Plasticity of *Streptomyces coelicolor* membrane composition under different growth conditions and during development, Frontiers in microbiology 6 (2015) 1465.

[31] A. Nishibori, J. Kusaka, H. Hara, M. Umeda, K. Matsumoto, Phosphatidylethanolamine domains and localization of phospholipid synthases in *Bacillus subtilis* membranes, Journal of bacteriology 187 (2005) 2163–2174.

[32] K. G. Kaval, S. Hauf, J. Rismondo, B. Hahn, S. Halbedel, Genetic dissection of DivIVA functions in *Listeria monocytogenes*, Journal of bacteriology 199 (2017) e00421–17.

[33] J. Rismondo, R. M. Cleverley, H. V. Lane, S. Großhennig, A. Steglich, L. Möller, G. K. Mannala, T. Hain, R. J. Lewis, S. Halbedel, Structure of the bacterial cell division determinant GpsB and its interaction with penicillin-binding proteins, Molecular microbiology 99 (2016) 978–998.

[34] D. H. de Jong, G. Singh, W. D. Bennett, C. Arnarez, T. A. Wassenaar, L. V. Schafer, X. Periole, D. P. Tieleman, S. J. Marrink, Improved parameters for the martini coarse-grained protein force field, Journal of Chemical Theory and Computation 9 (2012) 687–697.

Graphical Abstract

Effect of membrane composition on DivIVA-membrane interaction

Miroslav Jurásek,Klas Flärdh,Robert Vácha

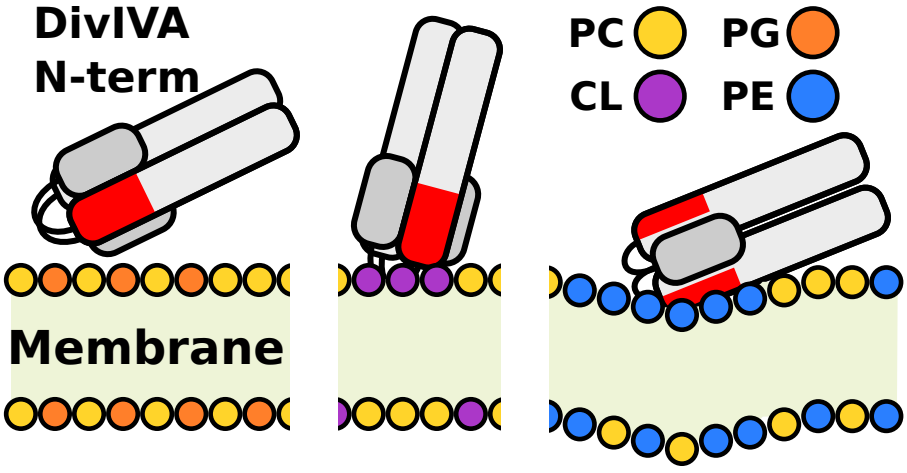

Highlights

Effect of membrane composition on DivIVA-membrane interaction

Miroslav Jurásek,Klas Flärdh,Robert Vácha

- Interaction between membranes with different lipid composition and DivIVA N-terminal domain from *Streptomyces coelicolor* was studied via MD simulations and compared to DivIVA N-terminal domain from *Bacillus subtilis*.
- Lipid composition influenced affinity of the DivIVA N-terminal domain towards the membrane and changed its orientation on the membrane.
- Strongest interaction was observed for ~~POPE~~phosphatidylethanolamine and cardiolipin, lipids which both posses preference for negatively ~~curvature~~curved membranes.

Supplementary Information
Effect of membrane composition on DivIVA-membrane interaction

Miroslav Jurásek[1], Klas Flärdh[1], Robert Vácha[1,1]

All-atom simulations

All-atom simulations were performed using CHARMM36 force-field [1] with standard TIP3 water model [2]. Simulations were performed in a NPT ensemble with periodic boundary conditions at temperature 309.15 K and pressure 1 bar. We employed a leap-frog integrator to solve equations of motion. The Verlet neighbor search with 0.005 kJ mol^{-1} ps^{-1} buffer was used. The temperature in the system was controlled by Nosé–Hoover thermostat[3, 4] with the time constant 1 ps and pressure was controlled via Parrinello-Rahman barostat[5] with a coupling time of 5 ps and a compressibility of 4.5×10^{-5} bar^{-1}. To avoid artificial temperature gradients, solute and solvent were coupled to thermostat separately. Isotropic pressure coupling was applied in simulations with protein in solution. In systems with membranes semiisotropic coupling was used with the pressure in the membrane normal and membrane plane coupled separately. Center of mass movement was removed separately for solvent and membrane with protein every 5 ps. Long-range electrostatics was calculated via PME[6, 7] with direct space cut-off 1.2 nm. Short range Van der Walls interactions were cut-off at 1.2 nm with force-shift applied from 1.0 nm. All hydrogen atoms bound to heavy atoms were constrained with LINCS [8].

Coarse-grained simulations

Coarse-grained simulations were carried out using Martini v2.2 force-field [9, 10, 11] with explicit Martini water and ions. Simulations were performed in NPT ensemble at temperature 320 K and pressure 1 bar with time step set to 20 fs employing the leap-frog integrator. The Verlet neighbor search with 0.005 kJ mol^{-1} ps^{-1} buffer was used. The temperature was controlled via velocity-rescale algorithm [12] with the time constant of 1.0 ps where the solute and solvent were coupled separately. Pressure was controlled with Parrinello-Rahman barostat [5] with the time constant of 12 ps. Compressibility was set to 30×10^{-5} bar^{-1}. Pressure coupling was applied isotropically with the exception of membrane systems where the pressure in membrane plane and membrane normal were coupled separately. Both Coulomb and van der Walls interactions were treated with simple cut-off at 1.1 nm. Interactions beyond cut-off were smoothly shifted to zero with the potential-shift-verlet algorithm [13], with isotropic permitivity $\epsilon_r = 15$. When placed on the membrane surface the N-terminal domain were restrained with the additional elastic network between Martini beads to maintain equlibrated protein structure. Elastic bonds were constructed by using default parameters: force constant was 500 kJ $mol^{-1}nm^{-1}$, and the lower and upper elastic bond cut-off was set to 0.5 and 0.9 nm, respectively. Martini simulations with the domain structure held by elastic bonds were denoted as rigid marked by R, otherwise, we denote them as flexible with F. Simulation times reported in the article are actual simulation times without accounting for Martini effective speedup of four times. [14]

System preparation

All initial membrane configurations were generated with CHARMM-GUI [15, 16, 17, 18]. Membranes were solvated in 150 mM aqueous solution of NaCl with additional ions to neutralize the system. Membranes were equilibrated till area per lipid (APL) converged to steady state (up to 50 ns). We investigated interactions between DivIVA N-terminal domain and following lipids: phosphatidylcholine (POPC), phosphatidylethanolamine (POPE), phosphatidylglycerol (POPG), tetramyristoylcardiolipin with charge -1 e (TMCL1), and tetraoleylcardiolipin with charge -2 e (TOCL2). We tested five different membrane lipid compositions: pure POPC and POPE, 1:1 POPE-POPC, 1:1 POPG-POPC, 20:7:3 POPE-POPG-TMCL1, 11:5:4 POPC-POPG-TOCL2. Each system consisted of 300 lipids with the exception of POPC-POPG-TOCL2 system with 320 lipids. Equal number of lipids were distributed in each leaflet.

The initial all-atom structure of the DivIVA(Scoel) N-terminal domain was taken from homology modeling. For Martini simulation, the model was coarse-grained using martinize script [19]. All proteins were solvated in explicit water with physiological 150 mM ion concentration and excess ions to neutralize systems. After equilibration, the

protein structures were combined with membrane systems in three steps. First, the solvent was removed from equilibrated structures of protein and membrane. Second, both protein and membrane were put together, so that protein and membrane were in close proximity with the protein aligned along the membrane normal. The N-terminal domain was oriented with the membrane interaction loop (domain tip – residues 16-21 in Scoel and 15-19 in Bsubt) facing the membrane. The orientation was chosen based on the reported preference of the loop residues for the membrane interaction. [20] In the third step, the whole system was solvated in a rectangular box of size 9.5 x 9.5 x 14 nm with $\approx$ 30 x 10^3 TIP3P water or 20.0 x 20.0 x 15.0 nm with $\approx$ 33 x 10^3 Martini water in AA and CG simulations,respectively. In both AA and CG systems NaCl salt with physiological 150 nM concentration was added together with excess ions to neutralize system charge. The exception was POPC-POPG-TOCL2 (CL2) membrane, where more water molecules $\approx$ 42 x 10^3 TIP3P water in a box of 11.2 x 11.2 x 14 nm or $\approx$ 41 x 10^3 Martini water in a box of 22.2 x 22.2 x 15.0 nm were used for AA or CG, respectively.

All protein-membrane systems were equilibrated for at least 80 ns. The exception~~was pure POPC membrane, which was equilibrated for 50 ns.~~s were: pure POPC membrane for Scoel variant, pure POPE membranes for both Scoel and Bsubt variants, and 1:1 POPG-POPC membrane for Bsubt variant, which were equilibrated for 50 ns, 10 ns, and 10 ns respectively. Production dynamics were 100 ns for all-atom simulations while in MARTINI we simulated the system for 2 μs with flexible domain and 1 μs for rigid domain. In Martini simulations, the domain was kept in a close proximity to the membrane with flat-bottom potential during the equilibration otherwise the domain tends to dissociate in first few ns. Each membrane composition was simulated in at least two copies which differed in initial membrane configuration to obtain better and independent sampling. [21] Exception was pure POPE membrane with the N-terminal domain from Scoel, where only one copy was simulated. The systems were analyzed independently and the conclusions were drawn based on the similarities between the systems. Analysis of orientation preference was done only from frames where the interaction between the membrane and the domain was stronger then 0 kJ mol^{-1}.

Supplementary Figures

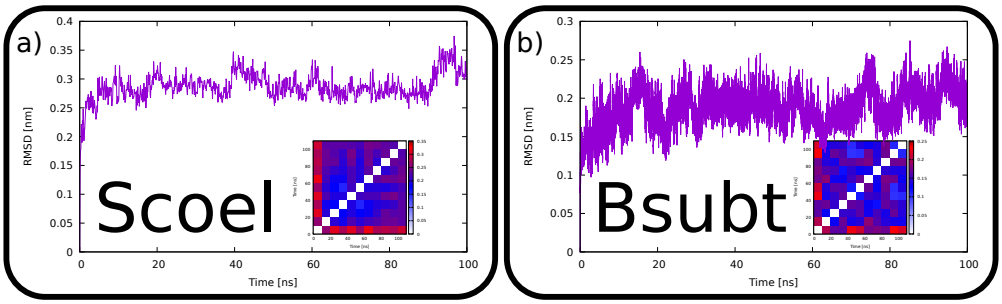

Figure S1: RMSD evolution of N-terminal domain a) homology model (Scoel) and b) N-terminal domain (Bsubt) simulated in free NPT simulations. System seems to equlibrate within first ~~10~~5 ns. Main source of structure fluctuations are from free ends.Insets show RMSD between snapshots taken at different times during the simulation. We can see that after initial change in RMSD the structures ~~is~~are stable and fluctuate within 0.15 nm.

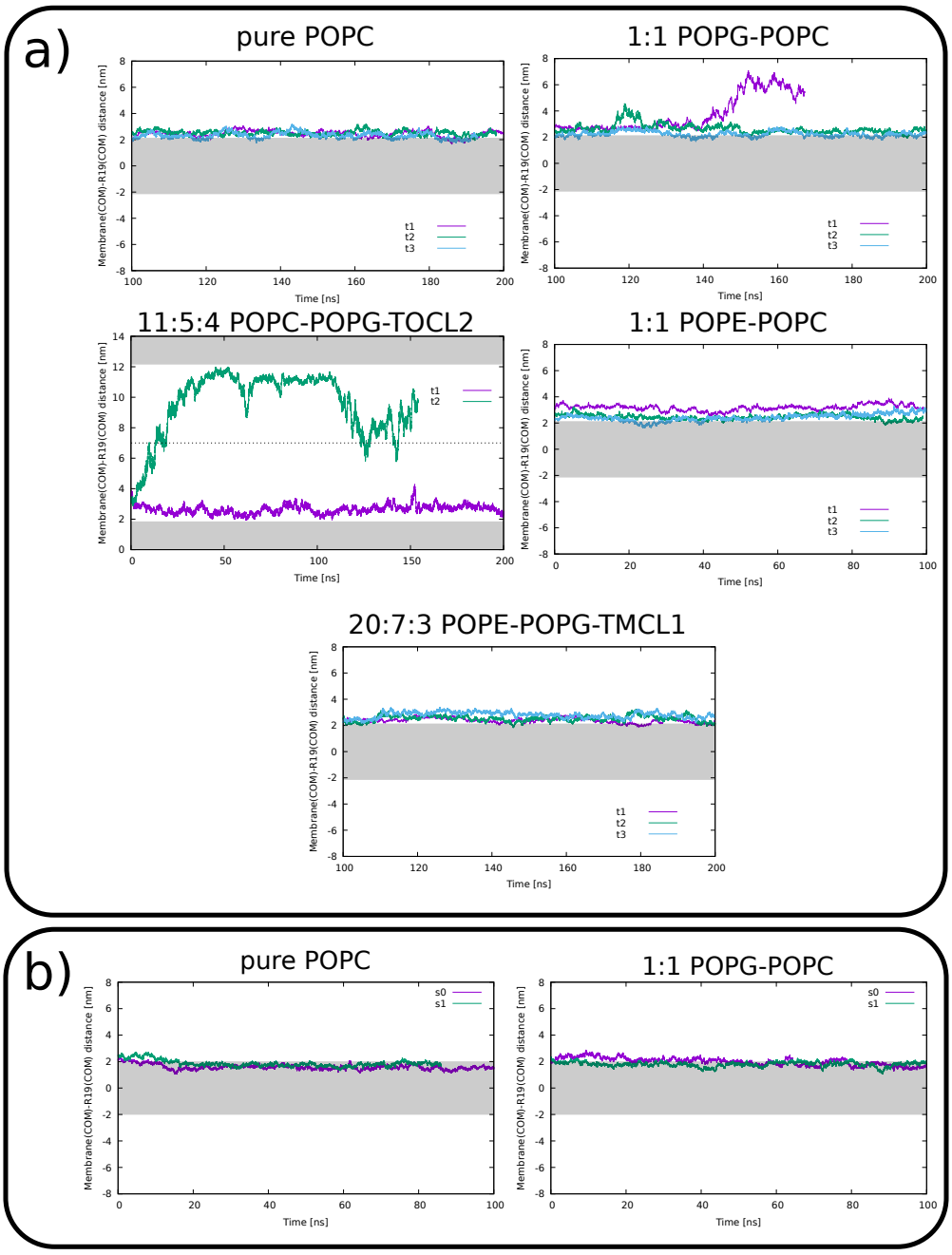

Figure S2: Distance between membrane center of mass and the N-terminal domain tip for different membrane compositions ~~(tip is defined as center of mass of two R19 residues)~~in the DivIVA protein from a) Scoel and b) Bsubt. Here the tip is defined by center of mass of two Arg 19 or two Phe 17 residues for Scoel or Bsubt variant, respectively. Rough position and width of the membrane is depicted with gray rectangle. Note that in 11:5:4 POPC-POPG-TOCL2 the domain in simulation t2 unbind and rebind to other side of the membrane. Thus both membrane leaflets are shown across the simulation box which boundary is depicted with dotted line.

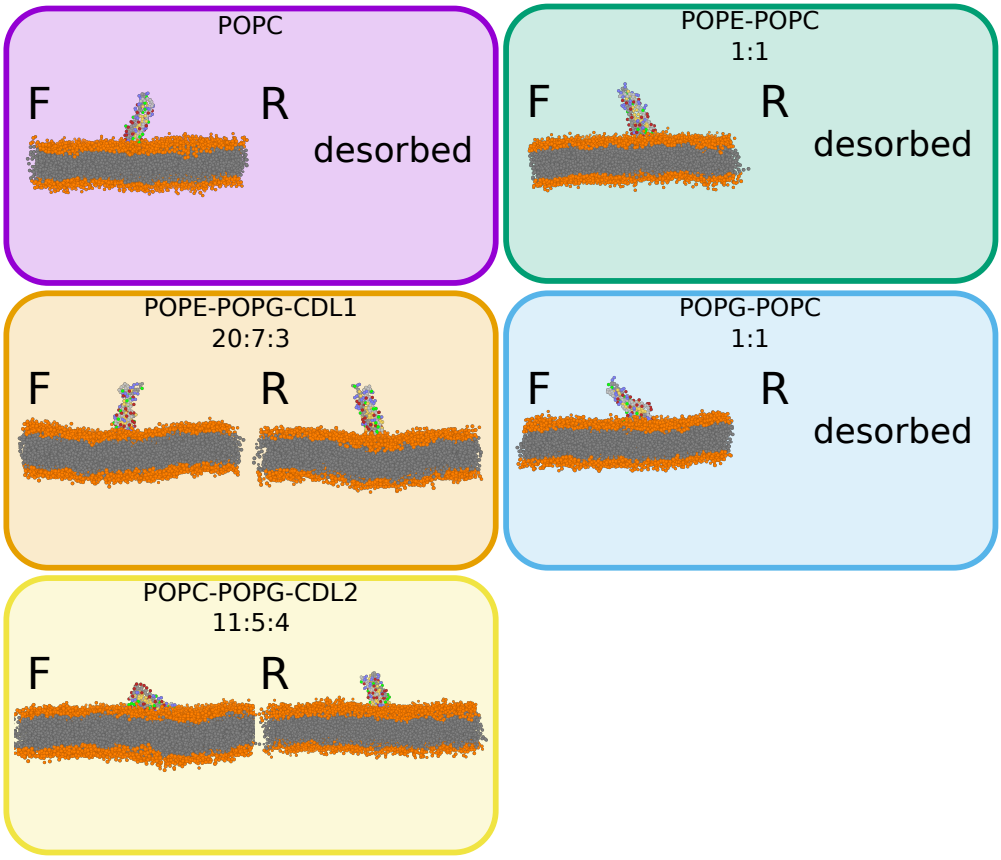

Figure S3: Final configuration of Martini simulations of N-terminal domain (Scoel) on different membrane compositions. Simulations with flexible and rigid domain are marked with F and R, respectively. For simulation where rigid domain did not adsorb to the membrane snapshots are missing. Note that in Martini force-field cardiolipin molecules with charge -2 e and -1 e are denoted as CDL1 and CDL2, respectively.

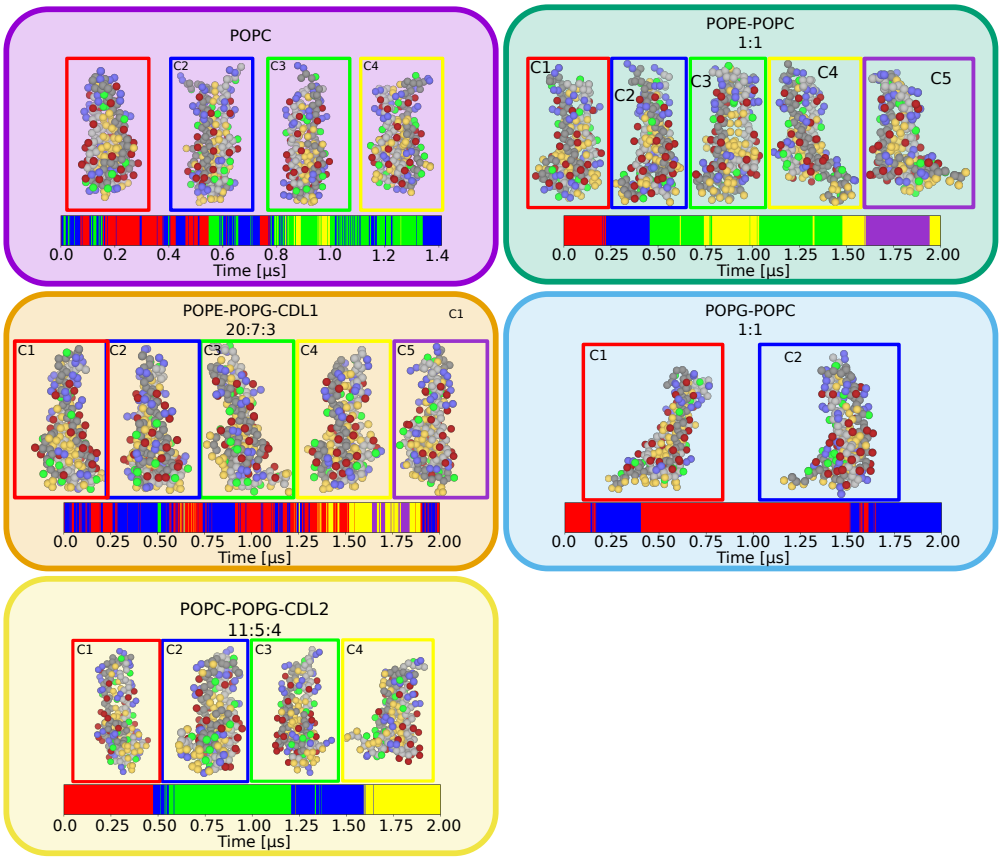

Figure S4: Clustered configurations of the flexible N-terminal domain (Scoel) that was adsorbed to the membrane surface. Clusters are ordered by time of their appearance that is depicted bellow. Each box corresponds to different membrane compositions. Cluster representative structures are shown in colored boxes with colors corresponding to colors in time line. Clusters are numbered base on first time occurrence of given cluster. Time evolution of the domain unfolding is shown below with colors corresponding to cluster colored frames. Note that in Martini force-field cardiolipin molecules with charge -2 e and -1 e are denoted as CDL1 and CDL2, respectively.

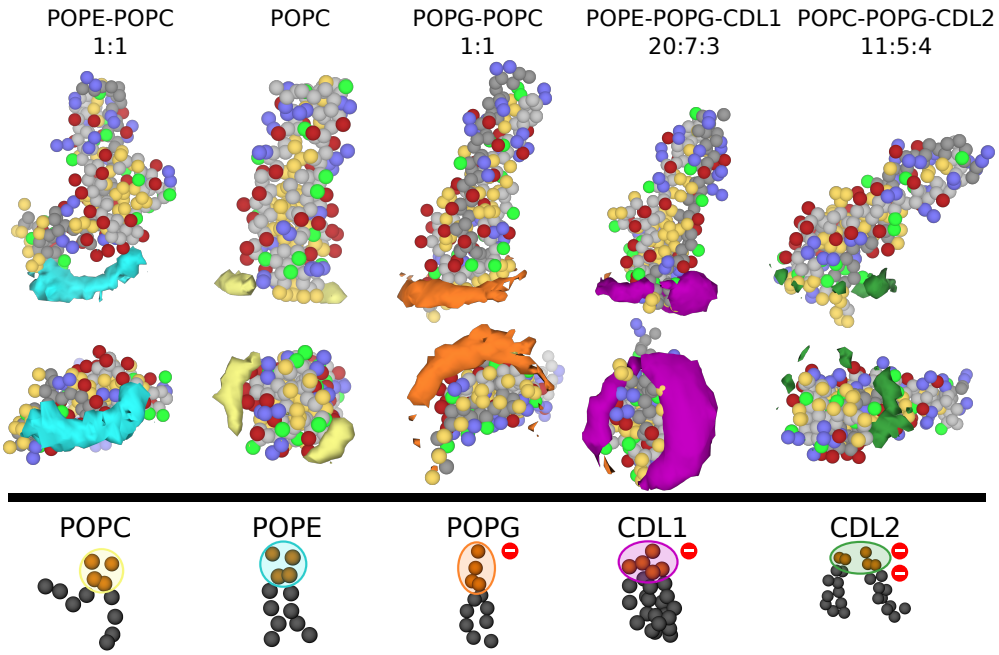

Figure S5: Lipid distribution around the flexible N-terminal domain (Scoel) in five different lipid compositions calculated with Martini force-field. Note that in Martini model TMCL1 and TOCL2 used in all-atom model are modeled as CDL1 and CDL2, respectively. The N-terminal domain is depicted with backbone in gray, where darker and lighter corresponds to chain A and B, respectively. Side chain beads are colored based on residue character: hydrophobic, polar, negatively, and positively charged are yellow, green, red, and blue, respectively. Note that in Martini force-field cardiolipin molecules with charge -2 e and -1 e are denoted as CDL1 and CDL2, respectively.

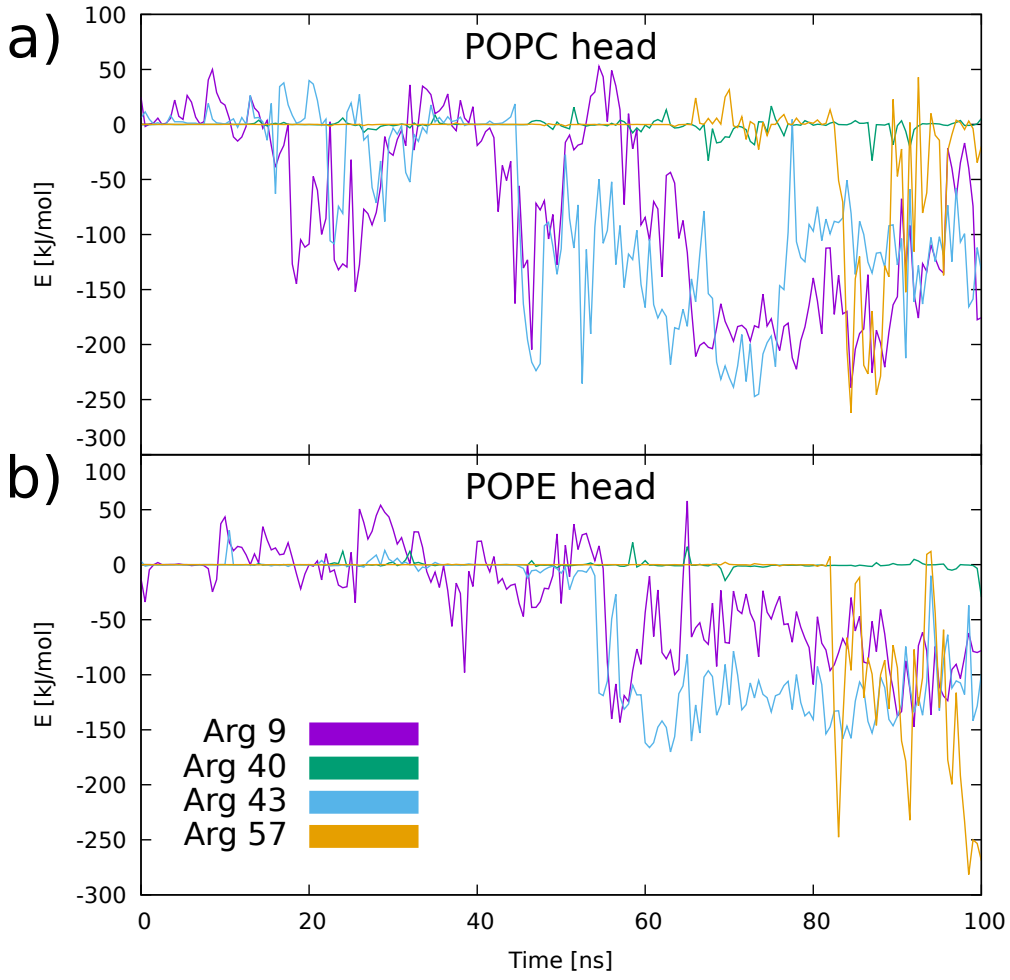

Figure S6: Time dependence of interaction energy between for a) POPC and b) POPE head-groups and all arginine residues (Arg 9, Arg 40, Arg 43, and Arg 57) except for the tip arginines (Arg 17 and Arg 19). ~~Data are derived for 1:1 POPC-POPE membrane~~Data from 1:1 POPE-POPC membrane with bound N-terminal domain (Scoel) from trajectory t1.

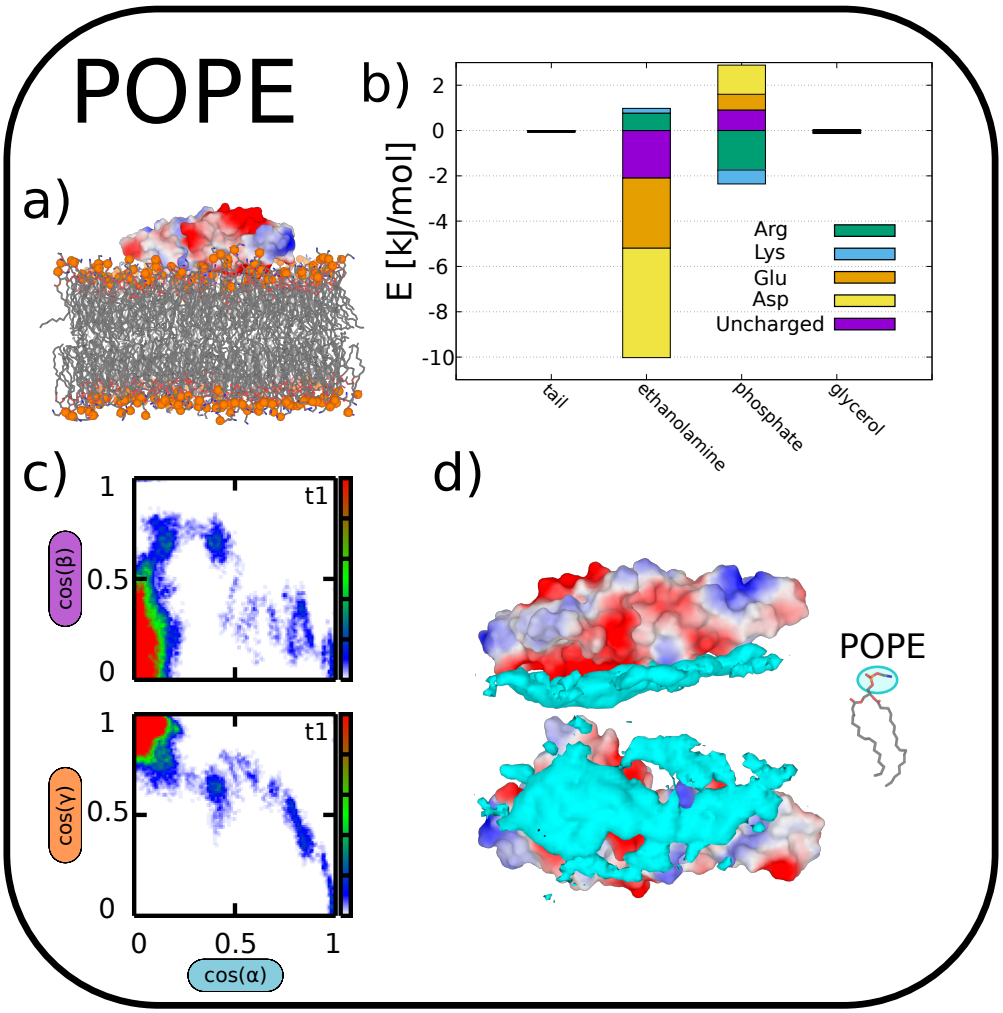

Figure S7: Interaction between the Scoel N-terminal domain and the pure POPE membrane. a) the final configuration of the 110 ns long simulation. b) an average interaction strength per one lipid between lipid moieties and the Scoel N-terminal domain. c) the Scoel N-terminal domain orientation on the membrane (for description of axis see Fig. 4). d) Average number density of POPE lipid head-groups around the N-terminal domain of Scoel.

References

[1] R. B. Best, X. Zhu, J. Shim, P. E. Lopes, J. Mittal, M. Feig, A. D. MacKerell Jr, Optimization of the additive CHARMM all-atom protein force field targeting improved sampling of the backbone ϕ, ψ and side-chain $\chi 1$ and $\chi 2$ dihedral angles, Journal of chemical theory and computation 8 (2012) 3257–3273.

[2] W. L. Jorgensen, J. Chandrasekhar, J. D. Madura, R. W. Impey, M. L. Klein, Comparison of simple potential functions for simulating liquid water, The Journal of chemical physics 79 (1983) 926–935.

[3] S. Nosé, A molecular dynamics method for simulations in the canonical ensemble, Molecular physics 52 (1984) 255–268.

[4] W. G. Hoover, Canonical dynamics: Equilibrium phase-space distributions, Physical review A 31 (1985) 1695.

[5] M. Parrinello, A. Rahman, Polymorphic transitions in single crystals: A new molecular dynamics method, Journal of Applied physics 52 (1981) 7182–7190.

[6] T. Darden, D. York, L. Pedersen, Particle mesh Ewald: An N log (N) method for Ewald sums in large systems, The Journal of chemical physics 98 (1993) 10089–10092.

[7] U. Essmann, L. Perera, M. L. Berkowitz, T. Darden, H. Lee, L. G. Pedersen, A smooth particle mesh Ewald method, The Journal of chemical physics 103 (1995) 8577–8593.

[8] B. Hess, H. Bekker, H. J. Berendsen, J. G. Fraaije, LINCS: a linear constraint solver for molecular simulations, Journal of computational chemistry 18 (1997) 1463–1472.

[9] S. J. Marrink, A. H. De Vries, A. E. Mark, Coarse grained model for semiquantitative lipid simulations, The Journal of Physical Chemistry B 108 (2004) 750–760.

[10] S. J. Marrink, H. J. Risselada, S. Yefimov, D. P. Tieleman, A. H. De Vries, The MARTINI force field: coarse grained model for biomolecular simulations, The journal of physical chemistry B 111 (2007) 7812–7824.

[11] L. Monticelli, S. K. Kandasamy, X. Periole, R. G. Larson, D. P. Tieleman, S.-J. Marrink, The MARTINI coarse-grained force field: extension to proteins, Journal of chemical theory and computation 4 (2008) 819–834.

[12] G. Bussi, D. Donadio, M. Parrinello, Canonical sampling through velocity rescaling, The Journal of chemical physics 126 (2007) 014101.

[13] M. J. Abraham, T. Murtola, R. Schulz, S. Páll, J. C. Smith, B. Hess, E. Lindahl, GROMACS: high performance molecular simulations through multi-level parallelism from laptops to supercomputers, SoftwareX 1 (2015) 19–25.

[14] H. I. Ingólfsson, C. A. Lopez, J. J. Uusitalo, D. H. de Jong, S. M. Gopal, X. Periole, S. J. Marrink, The power of coarse graining in biomolecular simulations, Wiley Interdisciplinary Reviews: Computational Molecular Science 4 (2014) 225–248.

[15] S. Jo, T. Kim, V. G. Iyer, W. Im, CHARMM-GUI: a web-based graphical user interface for CHARMM, Journal of computational chemistry 29 (2008) 1859–1865.

[16] S. Jo, J. B. Lim, J. B. Klauda, W. Im, CHARMM-GUI membrane builder for mixed bilayers and its application to yeast membranes, Biophysical journal 97 (2009) 50–58.

[17] E. L. Wu, X. Cheng, S. Jo, H. Rui, K. C. Song, E. M. Dávila-Contreras, Y. Qi, J. Lee, V. Monje-Galvan, R. M. Venable, J. Klauda B, W. Im, CHARMM-GUI membrane builder toward realistic biological membrane simulations, Journal of computational chemistry 35 (2014) 1997–2004.

[18] J. Lee, X. Cheng, J. M. Swails, M. S. Yeom, P. K. Eastman, J. A. Lemkul, S. Wei, J. Buckner, J. C. Jeong, Y. Qi, S. Jo, V. S. Pande, D. A. Case, C. L. Brooks, A. D. J. MacKerell, J. B. Klauda, W. Im, CHARMM-GUI input generator for NAMD, GROMACS, AMBER, OpenMM, and CHARMM/OpenMM simulations using the CHARMM36 additive force field, Journal of chemical theory and computation 12 (2015) 405–413.

[19] D. H. de Jong, G. Singh, W. D. Bennett, C. Arnarez, T. A. Wassenaar, L. V. Schafer, X. Periole, D. P. Tieleman, S. J. Marrink, Improved parameters for the martini coarse-grained protein force field, Journal of Chemical Theory and Computation 9 (2012) 687–697.

[20] M. A. Oliva, S. Halbedel, S. M. Freund, P. Dutow, T. A. Leonard, D. B. Veprintsev, L. W. Hamoen, J. Löwe, Features critical for membrane binding revealed by DivIVA crystal structure, The EMBO journal 29 (2010) 1988–2001.

[21] A. Grossfield, S. E. Feller, M. C. Pitman, Convergence of molecular dynamics simulations of membrane proteins, Proteins: structure, function, and bioinformatics 67 (2007) 31–40.